Supporting Information

Doc2-mediated superpriming supports synaptic augmentation

Renhao Xue[a,b], David A. Ruhl [a,b,c], Joseph S. Briguglio [a,b], Alexander G. Figueroa[d], Robert A. Pearce[d], and Edwin R. Chapman[a,b,1]

[a] Howard Hughes Medical Institute, University of Wisconsin–Madison, Madison, WI 53705-2275
[b] Department of Neuroscience, University of Wisconsin–Madison, Madison, WI 53705-2275
[c] Neuroscience Training Program, University of Wisconsin, Madison, WI 53705-2275
[d] Department of Anesthesiology, University of Wisconsin–Madison, Madison, WI 53705-2275

[1] To whom correspondence should be addressed. Email: chapman@wisc.edu
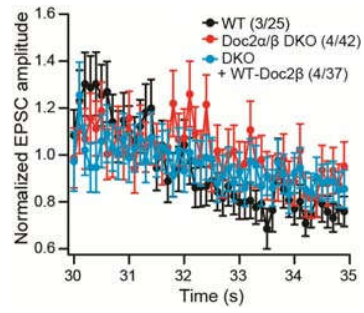
Fig. S1. Synaptic responses during the 10 Hz stimulus train. Normalized peak amplitudes of evoked EPSCs, recorded from cultured hippocampal neurons. All data are plotted as mean ± SEM. These data correspond to the grey bar in Fig. 1B.
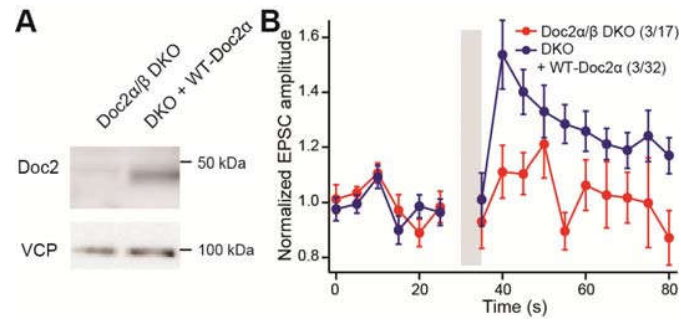
Fig. S2. Expression of Doc2α rescues synaptic augmentation in Doc2α/β DKO neurons. (**A**) Lysates of Doc2α/β DKO neurons with or without lentiviral expression of WT-Doc2α were subjected to SDS/PAGE and immunoblot analysis using an anti-Doc2 antibody. VCP was also blotted as a loading control. A representative blot, from three independent trials, is shown. (**B**) Augmentation was fully rescued by Doc2α. Normalized peak amplitudes of EPSCs before and after the augmentation protocol (grey bar, 10 Hz, 5 s), recorded from Doc2α/β DKO and DKO + WT-Doc2α neurons, are plotted versus time as in Fig. 1.
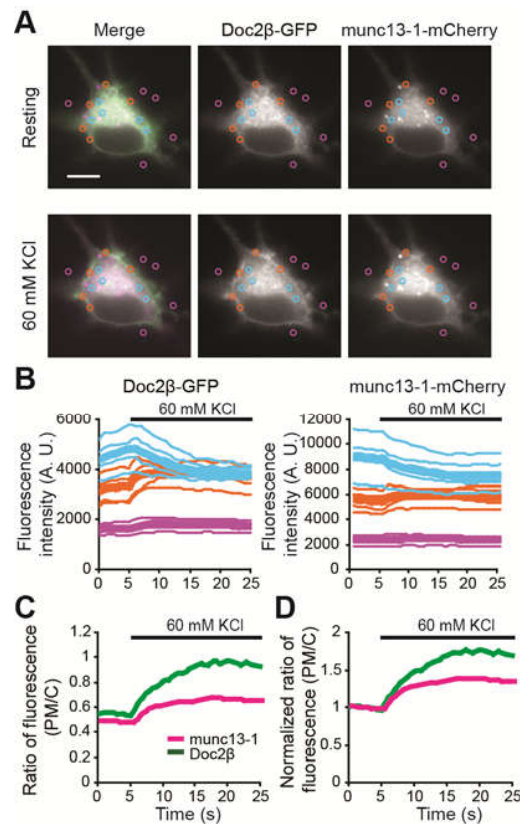
Fig. S3. Quantification of plasma membrane translocation of Doc2β-GFP and munc13-1-mCherry. (**A**) Five points located in the cytosol (cyan), five points on the plasma membrane (orange), and another five points in a non-cell area (pink) were randomly selected from each image stack for analysis. (**B**) The GFP (left) or mCherry (right) fluorescence intensities of these 15 individual points are plotted versus time (thin lines). The averaged fluorescence intensities of points in the cytosol (cyan, thick line), on the plasma membrane (orange, thick line), as well as the background signals (pink, thick line) are plotted versus time. (**C**) The ratios of averaged fluorescence intensities from the plasma membrane (PM) and cytosol (C) were calculated after subtracting the background. (**D**) Data from *panel C* were normalized to the average value of the baseline (the first five seconds).
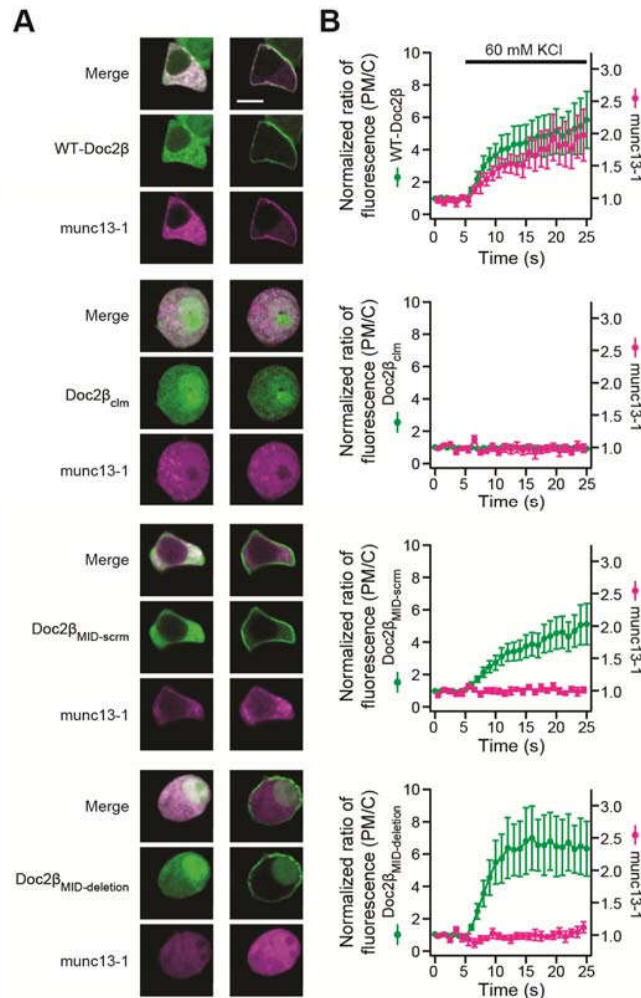
Fig. S4. Ca^{2+}•Doc2β mediates munc13-1 translocation to the plasma membrane in PC12 cells. (**A**) Representative images of PC12 cells before and after depolarization with 60 mM KCl: munc13-1-mCherry (magenta) and WT Doc2β-GFP (green) both translocate to the plasma membrane; Doc2β$_{clm}$-GFP neither translocates itself, nor recruits munc13-1-mCherry; Doc2β$_{MID-scrm}$-GFP and Doc2β$_{MID-deletion}$-GFP translocate without recruiting munc13-1-mCherry. These observations are consistent with the findings in the soma of neurons, as shown in Fig. 2; scale bar = 10 μm. (**B**) Translocation data from *panel A* were quantified and plotted, as detailed in Fig. S3. The mean ± SEM from six independent coverslips are plotted for each condition.
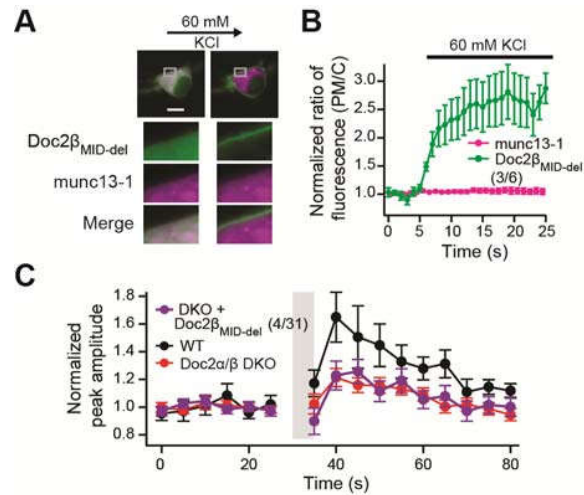
Fig. S5. Doc2β$_{MID-del}$ failed to recruit munc13 to plasma membrane in response to Ca^{2+}, or rescue augmentation. (**A**) Doc2β$_{MID-del}$-GFP translocated to the plasma membrane upon depolarization with 60 mM KCl but was unable to induce translocation of munc13-1-mCherry; scale bar = 10 μm. (**B**) Translocation data from *panel A* were quantified and plotted. (**C**) Normalized peak EPSC amplitudes before and after the augmentation protocol are plotted as mean ± SEM versus time. Doc2β$_{MID-del}$ failed to rescue synaptic augmentation.
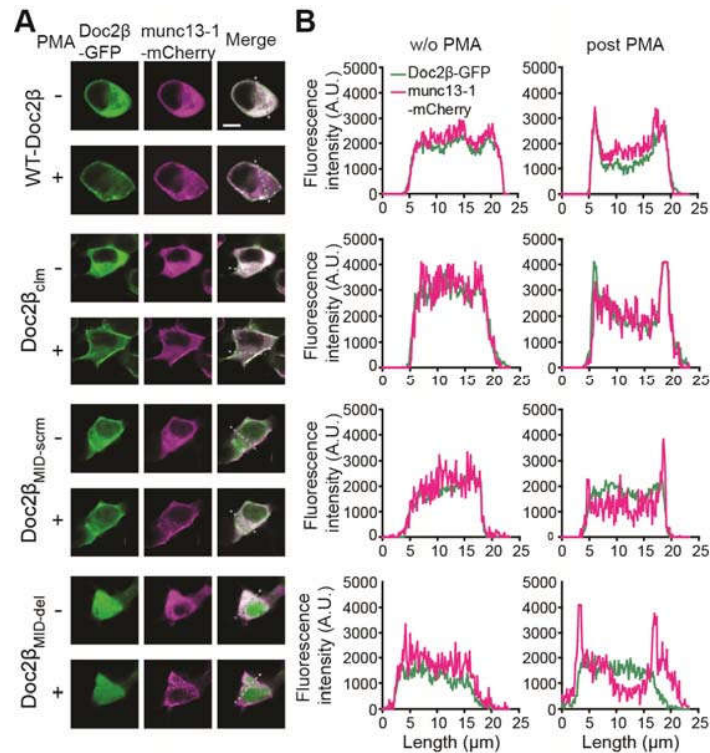
Fig. S6. Phorbol ester induced plasma membrane translocation of munc13-1 and MID-dependent recruitment of Doc2β. (**A**) When expressed in HEK293T cells, munc13-1-mCherry translocates to the plasma membrane after treatment with 0.1 μM PMA for 5 min. GFP tagged WT-Doc2β and Doc2β$_{clm}$ co-translocate together with munc13-1, whereas Doc2β$_{MID-scrm}$ and Doc2β$_{MID-del}$ are unable to co-translocate. For each condition, a representative cell from at least six independent coverslips is shown; scale bar = 10 μm. (**B**) Representative line scans of GFP and mCherry fluorescence (white lines in *panel A*) from HEK293T cells before and after treatment with PMA.
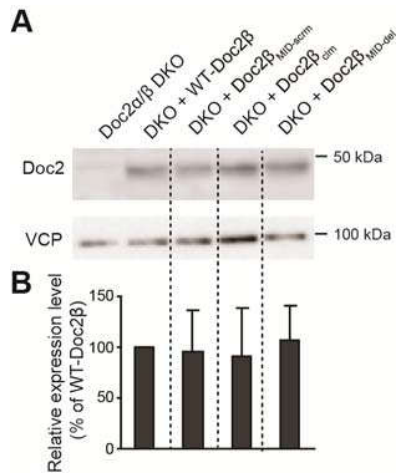
Fig. S7. Expression of Doc2β constructs in Doc2α/β DKO neurons. (**A**) Lysates from Doc2α/β DKO neurons expressing WT or the indicated mutant forms of Doc2β were subjected to SDS/PAGE and immunoblot analysis using an anti-Doc2 antibody. VCP was also blotted as a loading control. A representative blot, from three independent trials, is shown. (**B**) The expression levels of mutant forms of Doc2β were quantified as percentage of WT-Doc2β, and plotted as mean ± SEM (n = 3).
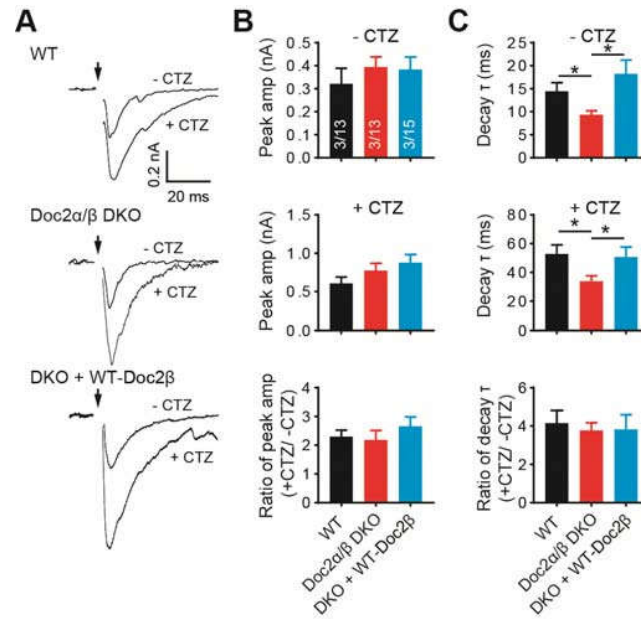
Fig. S8. Effect of Doc2 on EPSC decay kinetics does not involve postsynaptic receptor desensitization. (**A**) Representative evoked EPSC traces recorded from WT, Doc2α/β DKO, and DKO neurons expressing WT-Doc2β, in absence or presence of 100 µM CTZ, an inhibitor of AMPA receptor desensitization. (**B**-**C**) The EPSC peak amplitude (amp; **B**) and decay time constants (τ, calculated by exponential fitting; **C**) are represented as mean ± SEM. Consistent with Fig. 4, in the absence of CTZ (-CTZ, upper panels), no difference was found in peak amplitude while DKO of Doc2α/β significantly reduced the decay time constant, which was fully rescued by expression of WT-Doc2β. In the presence of CTZ (+CTZ, middle panels), the same trend was observed. The ratios of peak amplitudes and decay time constants (+CTZ/ -CTZ) were plotted as mean ± SEM in the lower panel. The effects of CTZ on WT, Doc2α/β DKO, and DKO neurons expressing WT-Doc2β were similar. * P<0.05, Kruskal–Wallis test followed by Dunn's post hoc test.
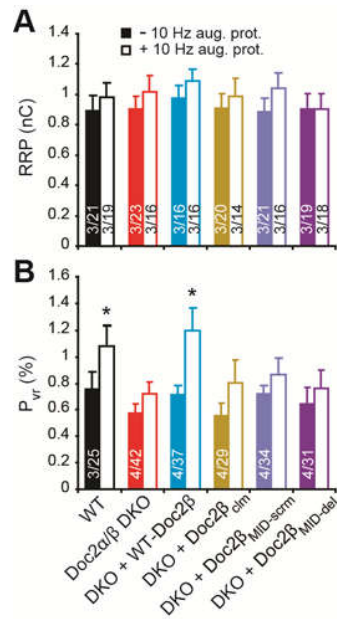
Fig. S9. Quantification of RRP size and P_{vr} from the hypertonic sucrose experiments. (**A**) RRP size was evaluated by integrating the charge transfer during the application of sucrose. (**B**) P_{vr} was calculated by normalizing the total charge of evoked EPSCs (Fig. 1) to the size of the RRP under each condition. Results from resting neurons (filled bars) or neurons after the 10 Hz augmentation protocol (open bars) are plotted as mean ± SEM. * P<0.05 versus Doc2α/β DKO, Kruskal–Wallis test followed by Dunn's post hoc test. The ratios of RRP and P_{vr} are shown in Fig. 5.
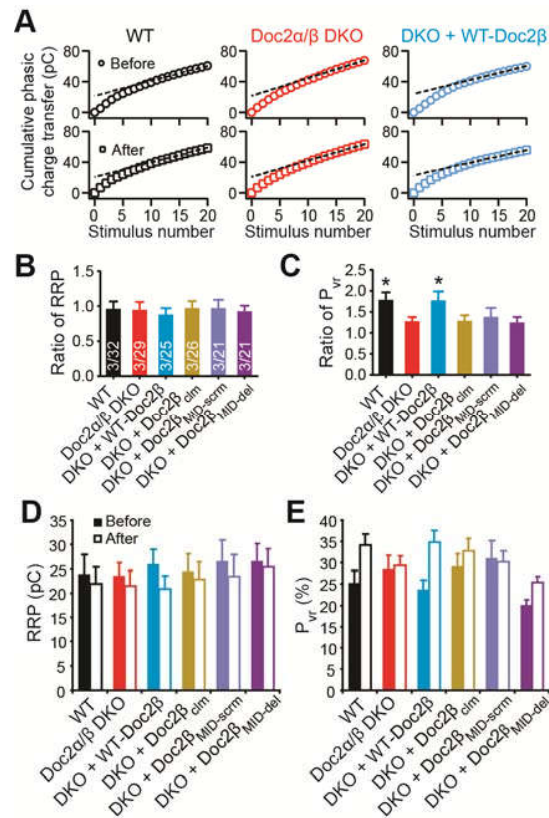
Fig. S10. Quantification of RRP size and P_{vr} from train stimulation data. (**A**) Cumulative phasic charge transfer during the two 40 Hz trains, before (open circle) and after (open square) the augmentation stimulus train (10 Hz, 5 s) are plotted versus time. The RRP size was determined by the y-intercept of the linear fit for data points 16 to 20 (steady state). (**B**) The RRP ratio was calculated by dividing RRP values obtained with and without augmentation. No significant differences were detected among each group (Kruskal–Wallis test). (**C**) P_{vr} was calculated by normalizing the charge of first EPSC peak to the RRP size. The P_{vr} ratio (P_{vr} after augmentation/ P_{vr} before augmentation) is plotted as mean ± SEM. (**D**-**E**) The original data of RRP size (**D**) and P_{vr} (**E**) are shown as mean ± SEM. * $P<0.05$ versus Doc2α/β DKO, Kruskal–Wallis test followed by Dunn's post hoc test.